ACSNANO
www.acsnano.org
ARTICLE

Piezotronic Effect Enhanced Photocatalysis in Strained Anisotropic ZnO/TiO_2 Nanoplatelets *via* Thermal Stress

Longfei Wang,[†,‡] Shuhai Liu,[†,‡] Zheng Wang,[§] Yongli Zhou,[†] Yong Qin,*[,†,§] and Zhong Lin Wang*[,†,⊥]

[†]Beijing Institute of Nanoenergy and Nanosystems, Chinese Academy of Sciences; National Center for Nanoscience and Technology (NCNST), Beijing 100083, China

[§]Institute of Nanoscience and Nanotechnology, School of Physical Science and Technology, Lanzhou University, Gansu 730000, China

[⊥]School of Material Science and Engineering, Georgia Institute of Technology, Atlanta, Georgia 30332, United States

Supporting Information

ABSTRACT: **Effective piezoelectric semiconductor based hybrid photocatalysts are successfully developed by assembling TiO_2 nanoparticles on ZnO monocrystalline nanoplatelets. The piezopotential can be introduced and tuned by thermal stress on the piezoelectric material of ZnO monocrystalline nanoplatelets through cooling hybrid photocatalysts from high temperature to room temperature with different rates based on the mismatched thermal expansion coefficient of the two materials, which can be used to engineer the heterojunction band structure and significantly enhance the photocatalytic performance in a wide range by improving charge separation. It is proposed that the piezotronic effect enhanced photocatalyst will provide a strategy for high-performance photocatalysis applications.**

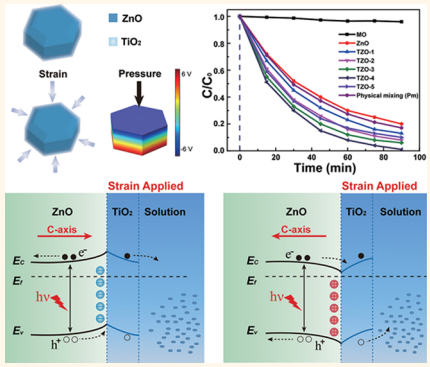

KEYWORDS: *photocatalysis, ZnO/TiO_2 heterojunction, piezoelectric, piezotronic effect, nanoplatelet*

Industrial wastewater contains a large amount of harmful organic compounds, especially all kinds of dyes,[1] which is challenging the quality of our life. Photocatalysis provides a potential strategy to decompose contaminants because it is a light-driven chemical process over the surface of a photocatalyst.[2,3] TiO_2, as the most prominent and suitable material for solar energy harvesting, is also widely studied in photocatalysis for the removal of inorganic and organic pollutants.[4,5] However, there are two basic problems that limit its further industrial applications. One problem is that it has a wide band gap of 3.2 eV, which limits its activity to the visible and infrared region.[6,7] The other problem is that most of the photogenerated electrons and holes will recombine, resulting in a relatively low photocatalytic efficiency. To solve these problems, on one hand, considerable efforts have been devoted to design effective photocatalysts for the full solar light spectrum.[8,9] Up to now, researchers have synthesized several photocatalysts for energy conversion and organic pollutant degradation with better utilization of solar energy. On the other hand, various methods have been used to try to promote the separation of photogenerated electrons and holes, such as using a cocatalyst and manufacturing heterostructures and photoelectrocatalysis systems.[10−12] Although the heterojunctions can improve the separation of photogenerated electrons and holes to some extent, the overall separation efficiency of electron and hole pairs is relatively low. So a bias field is applied on the film-like photoanode and Pt electrode in photoelectrocatalysis to more effectively separate the photoinduced electrons and holes.[13,14] However, the applied electric field consumes external electric power, and expensive platinum electrodes are necessary. At the same time, the photocatalyst is coated only on the surface of the electrode, which leads to the lack of enough surface area to absorb sufficient light and react, so that it is difficult to make a large-scale practical application for wastewater treatment. Hence, developing advanced technologies to highly efficiently separate the electrons and holes within semiconductors is still one of the great challenges for high-performance photocatalytic materials.

In recent years, internal electric fields from ferroelectric materials have been used to separate photoinduced carriers and to control the spatial location successfully in photovoltaic devices and photochemical reactivity by controlling local electronic structure.[15] When light is absorbed in the ferro-

Received: December 6, 2015
Accepted: January 8, 2016

DOI: 10.1021/acsnano.5b07678
ACS Nano XXXX, XXX, XXX−XXX

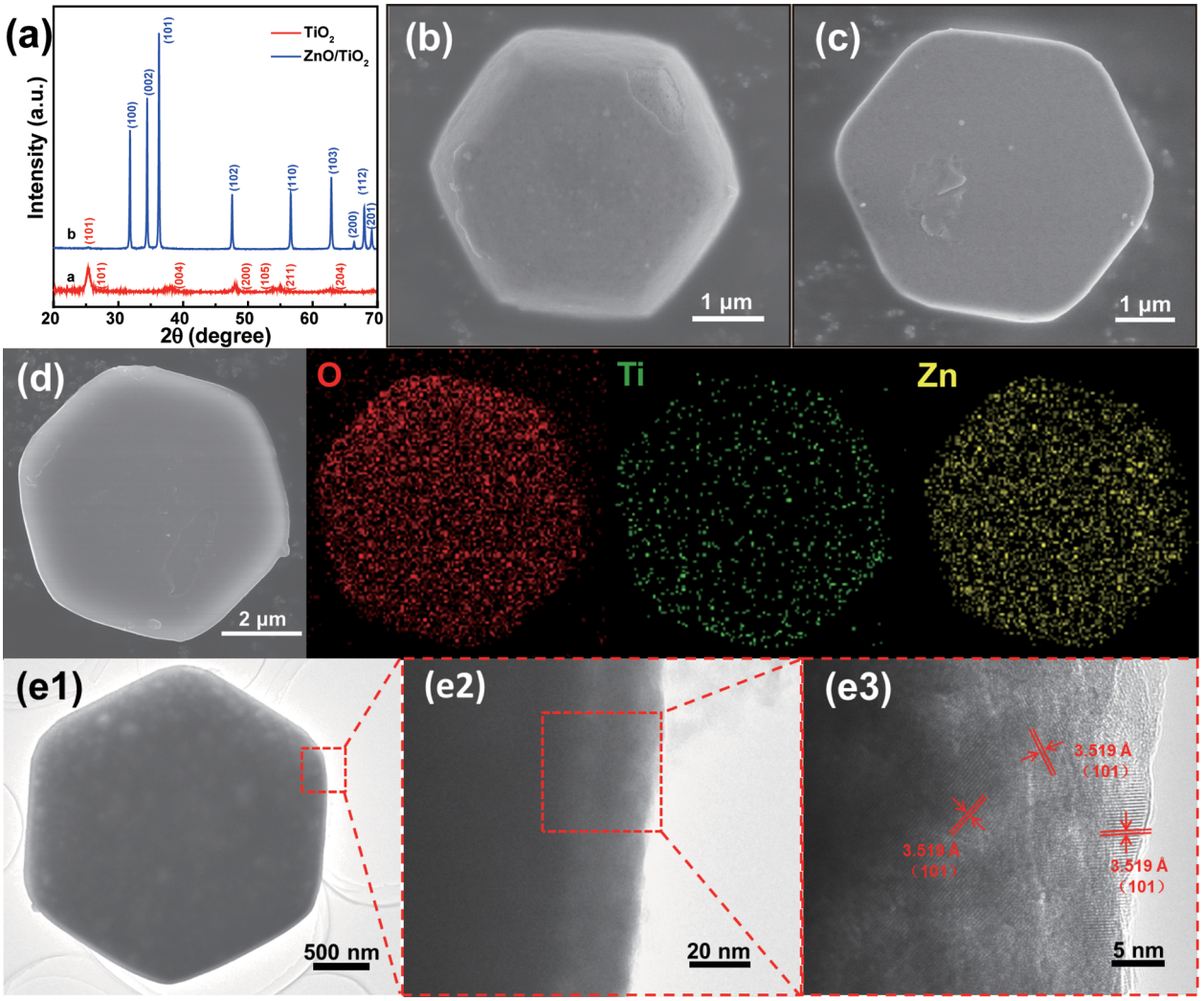

Figure 1. Structure and morphology of the ZnO/TiO_2 hybrid sample. (a) XRD patterns of the TiO_2 and ZnO/TiO_2 hybrid sample; (b, c, d) SEM images of a single ZnO/TiO_2 hybrid sample and the corresponding mapping results; (e1, e2) TEM images of a uniform ZnO/TiO_2 hybrid sample at different magnifications; (e3) HRTEM image of a ZnO/TiO_2 hybrid sample.

electric compounds, the built-in field provides a driving force for separating the photogenerated electrons and holes and thus enhancing the performance of photochemical reactivity. However, these ferroelectric materials are not ideal choices for photocatalysis because they have a wide band gap and low conductivity, the same as an insulator. Instead, piezoelectric semiconductors such as wurtzite ZnO have much higher conductivities, offer a balance between piezoelectric polarization and charge transport properties, and could serve as good candidates in the design of piezoenhanced photocalytic materials.[16,17] The concept of piezotronic effect was first proposed in 2007; this effect can modulate the electrical transporting property using the piezoelectric polarization charge induced inner-crystal potential in piezoelectric semiconductors at the semiconductor heterojunction or metal–semiconductor contacts.[18,19] This piezotronic effect has inspired the invention of many electronic and optoelectronic devices in the field of light-emitting diodes, solar cells, nanobots, and self-powered nanosystems.[20−25] It has been demonstrated that the photocurrent of a ZnO-based piezoelectric photoelectrochemical cell can be regulated, when the ZnO-based piezoelectric photoelectrochemical anode is under strain.[26] However, in this work, the surface area of the photocatalyst is too small to absorb sufficient light, and it requires a continuous application of an external mechanical force, which limits its large-scale applications for energy conversion and pollutant decomposition. From past reports, nanoplatelets have strong shape anisotropy and are easy to align.[27,28] Meanwhile, modulating strain in a semiconductor by thermal sintering has been widely used,[29,30] which makes it possible to induce anisotropic strain in nanoplatelets through sintering and cooling. So in this paper, we developed a kind of hybrid photocatalyst with anisotropic strain inside by assembling TiO_2 nanoparticles on ZnO monocrystalline nanoplatelets. On introducing strain, the piezopotential created by piezoelectric polarization charges presented at the ZnO/TiO_2 heterojunction interface effectively tune/control the charge transport across the interface/junction and modulate the optoelectronic processes of local carriers. Thus, the piezopotential of ZnO monocrystalline nanoplatelets can be used as a driving force to promote the separation of photogenerated carriers effectively *via* engineering the band structure of the ZnO/TiO_2 heterojunction interface. Through cooling the hybrid photocatalysts from high temperature with different rates, a piezopotential would be introduced and modulated through thermal stress created residual strain, since

DOI: 10.1021/acsnano.5b07678
ACS Nano XXXX, XXX, XXX−XXX

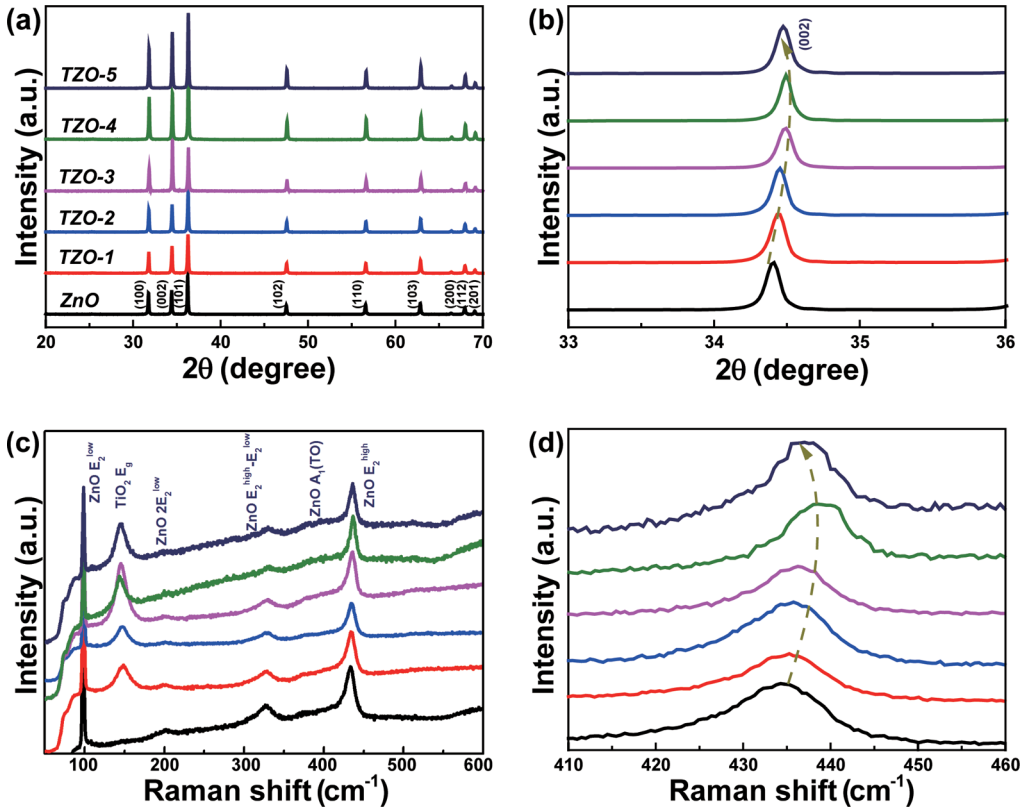

Figure 2. (a and b) General and high-precision XRD patterns of the samples: ZnO monocrystalline nanoplatelets, TZO-1, TZO-2, TZO-3, TZO-4, and TZO-5, respectively. (c and d) General and high-precision Raman spectra of the samples, respectively.

the thermal expansion coefficients of the two materials are mismatched. Comprehensive experimental results prove that the piezotronic effect can continuously enhance the photocatalytic performance of the ZnO/TiO_2 hybrid photocatalyst in a wide range. This study shows the potential of piezotronics for high-performance photocatalysis applications.

RESULTS AND DISCUSSION

To enhance the photocatalysis property by the piezotronic effect, suitable sized ZnO monocrystalline nanoplatelets and highly efficient photocatalyst TiO_2 nanoparticles were selected to assemble the heterojunction. The crystalline phase and morphology of the ZnO monocrystalline nanoplatelets were studied by powder X-ray diffraction (XRD), Raman scattering, scanning electron microscope (SEM), and high-resolution transmission electron microscope (HRTEM) (Figure S1, Supporting Information). The ZnO/TiO_2 hybrid samples were synthesized *via* a coprecipitation approach. A detailed discussion of the process is provided in the Supporting Information. The XRD patterns (Figure 1a) and X-ray photoelectron spectroscopy (XPS) spectra (Figure S2, Supporting Information) of the samples confirm that the ZnO/TiO_2 hybrid structure consists of hexagonal ZnO monocrystalline nanoplatelets (JCPDS No. 36-1451) and anatase TiO_2 (JCPDS No. 21-1272) nanoparticles. The hexagonal ZnO monocrystalline nanoplatelets are fully decorated with TiO_2 nanoparticles, as shown in the SEM (Figure 1b,c) and TEM (Figure 1e) images. Furthermore, the HRTEM image from the heterostructures shows a lattice spacing of 0.352 nm, corresponding to the (101) plane of the anatase crystal structure of TiO_2. In addition, the energy dispersive X-ray spectrometry (EDS) mapping (Figure 1d) images of a ZnO/TiO_2 hybrid product clearly show the uniform distribution of individual elements of O, Ti, and Zn, further confirming that the TiO_2 nanoparticles are uniformly assembled on the surface of the ZnO monocrystalline nanoplatelets.

In order to study the modulation effect of the cooling rate of hybrid photocatalysts on the residual strain, ZnO/TiO_2 hybrid powders were sintered at 450 °C for 2 h in a muffle furnace and then cooled in different processes. The sample naturally cooled in the muffle furnace from 450 °C to room temperature was named TZO-1, and the samples directly taken from the furnace at 450 °C after sintering and cooled to room temperature in air, in ice, and in liquid nitrogen were named TZO-2, TZO-3, and TZO-4, respectively. TZO-4 was further sintered at 200 °C and naturally cooled to room temperature to relieve the stress, and then it was named TZO-5. The phase purity and degree of crystallization for the as-synthesized samples are not obviously affected under different cooling conditions, as shown in the XRD spectra (Figure 2a) and from Raman spectroscopy (Figure 2c). From Figure 2b, the X-ray diffraction peak position exhibits a regular shift to higher degree from ZnO monocrystalline nanoplatelets to TZO-4 hybrids, while a reverse trend of shift in the peak position is observed from TZO-4 hybrids to TZO-5, which demonstrates that the samples have suffered different magnitudes of compressive strain along the *c*-axis direction. Furthermore, the compressive strain increases with the cooling rate and decreases gradually when the cooling rate decreases again. The above change of compressive strain in different ZnO/TiO_2 hybrid powder samples is also confirmed by the systematic shift of the E_2^{high} Raman peak position in Figure 2d. In order to further demonstrate the piezoelectric effect of ZnO monocrystalline nanoplatelets when the *c*-axis

DOI: 10.1021/acsnano.5b07678
ACS Nano XXXX, XXX, XXX−XXX

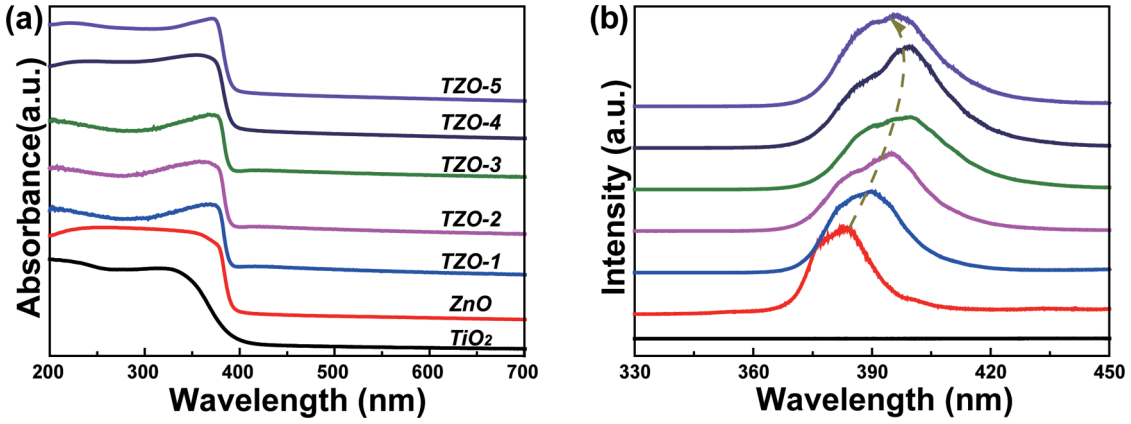

Figure 3. (a) Diffused reflectance UV spectra of the as-synthesized samples collected in the absorbance mode: TiO_2 nanoparticles, ZnO monocrystalline nanoplatelets, TZO-1, TZO-2, TZO-3, TZO-4, and TZO-5. (b) Photoluminescence spectra of as-synthesized samples recorded at an excitation wavelength of 365 nm and room temperature.

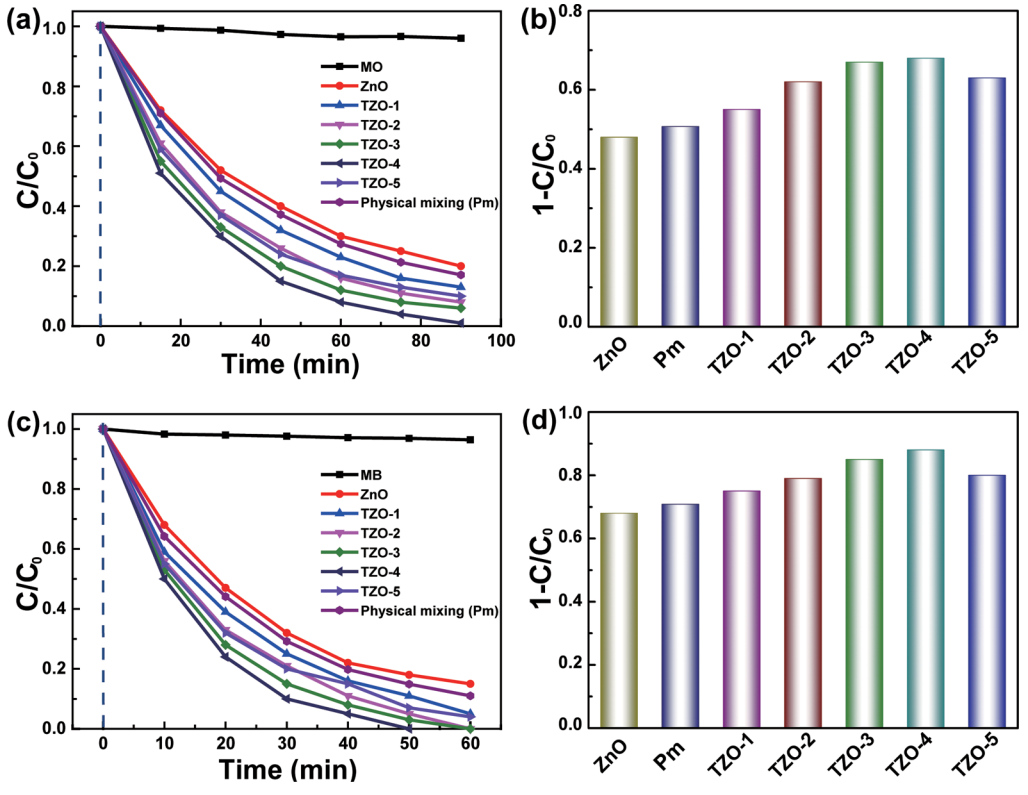

Figure 4. (a, c) Photocatalytic degradation of MO and MB as a function of irradiation time for photocatalysis in the presence of annealed ZnO monocrystalline nanoplatelets, TZO-1, TZO-2, TZO-3, TZO-4, and TZO-5 hybrid photocatalysts, a physical mixture of ZnO and TiO_2 powder, and self-degradation without catalyst. (b, d) Degradation efficiency of MO and MB in the presence of corresponding samples for 30 min.

undergoes compressive stress, the piezoelectric coefficient d_{33} of ZnO monocrystalline nanoplatelets was characterized, and single ZnO monocrystalline nanoplatelet nanogenerators (NGs) have been fabricated and measured (Figures S3a, S4, and S5, Supporting Information). The result illustrates that the piezoelectric coefficient d_{33} of ZnO monocrystalline nanoplatelets is about 22.5 pC/N, which is higher than that of the ZnO nanowire (Figure S6, Supporting Information). The linear correlation between the piezoelectric potential intensity and the strain was simulated using the COMSOL program (Figure S7, Supporting Information), which shows that even small strain can also produce considerable piezopotential. Therefore, it is effectively evident that we can introduce and modulate the piezoelectric potential by regulating residual strain *via* cooling samples from high temperature at different rates.

Subsequently, we explored the optical properties of samples with different residual strain in detail. The UV−vis absorption spectra of ZnO monocrystalline nanoplatelets, TiO_2 nanoparticles, and TZO-1, TZO-2, TZO-3, TZO-4, and TZO-5 hybrids are shown in Figure 3a. The TiO_2 nanoparticles have an intense absorption band with a steep edge at about 390 nm, which means the band gap is about 3.18 eV, and a higher deep UV region below 300 nm is observed. ZnO monocrystalline nanoplatelets and all TZO samples have strong adsorption in

DOI: 10.1021/acsnano.5b07678
ACS Nano XXXX, XXX, XXX−XXX

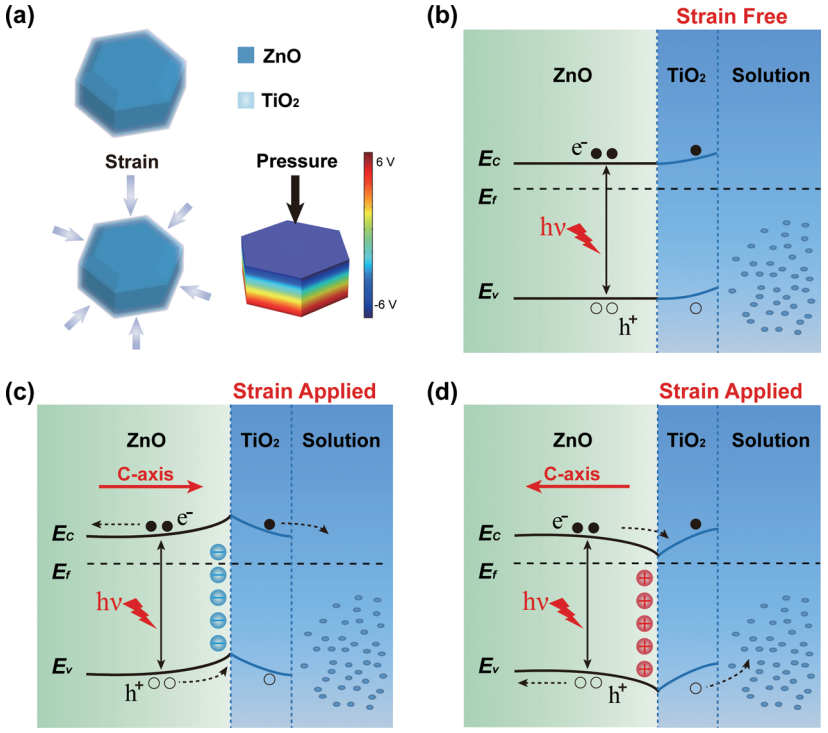

Figure 5. Piezotronics and the working mechanism of ZnO/TiO_2 hybrid photocatalysts. (a) 3D schematic demonstration of ZnO/TiO_2 hybrids without (top) and with strain (bottom left). Piezopotential distributions in a ZnO nanoplatelet (hexagonal edge: 2 μm, height: 1.5 μm) under an axial pressure of 10 MPa, simulated by a finite-element analysis method (COMSOL) (bottom right). Schematic band diagrams of ZnO/TiO_2 heterojunction without (b) and with (c, d) strain.

the UV region with an absorption edge at about 385 nm, which corresponds to the ZnO's band gap of 3.22 eV. For all TZOs, an absorbance below 300 nm ensures that the TiO_2 nanoparticles attached to ZnO monocrystalline nanoplatelets dominate the deep UV absorption. This may enhance their utilization of UV light compared with pure TiO_2 and ZnO monocrystalline nanoplatelets. Even though there are no significant changes in UV–vis absorption spectra, the absorption edge between each TZO sample shows an obvious shift. This result may be due to the strain when the samples are cooled at different rates, which is also proved by photoluminescence (PL) spectra of the samples. From the ZnO monocrystalline nanoplatelets to the sample of TZO-4, their PL spectra show a systematic red shift of the peak position (Figure 3b). On the contrary, from the TZO-4 to TZO-5 hybrid photocatalyst, a reverse trend of blue shift is observed in Figure 3b. It demonstrates that the band structure of ZnO/TiO_2 heterojunction's interface can be continuously engineered by the residual strain through cooling samples with different rates. A blue shift in the PL peak induced by pressure has been reported,[31−34] whereas we observed a systematic red shift, which indicates that the nonpolar surface of ZnO monocrystallines have also suffered compressive stress. This result is consistent with a previous report on red shift in the PL peak by Bin et al.[35]

To demonstrate the piezotronic effect on photocatalytic activity of ZnO/TiO_2 hybrids, we examine the photodegradation of methyl orange (MO) and methylene blue (MB) dye in solution with ZnO monocrystalline nanoplatelets, TZO-1, TZO-2, TZO-3, TZO-4, and TZO-5 hybrids, and a ZnO–TiO_2 physical mixture (optimized ratio of ZnO nanoplatelets and TiO_2 nanoparticles mixed together) under UV light irradiation as a function of time. In order to confirm the photodegradation of MO and MB dye is not caused by photolysis, we carried out all degradation experiments under UV light irradiation without catalyst. As expected, no obvious degradation of MO or MB dye can be detected, as shown in Figure 4a and c. Furthermore, a detailed analysis of MO photodegradation is carried out as follows. Compared with ZnO monocrystalline nanoplatelets and a ZnO–TiO_2 physical mixture, the TZO-1 sample has stronger photodegradation activity during the 90 min photocatalysis process. This improvement could be ascribed to a ZnO/TiO_2 heterojunction, which can separate the photogenerated carriers and decrease the electron–hole pair's recombination to some extent. More significantly, it is evident that the photocatalytic activity has strengthened gradually from TZO-1 to TZO-4 hybrid photocatalyst as the residual strain and piezoelectric potential of the sample increased; in contrast, a weakened photocatalytic activity can be observed from the TZO-4 to TZO-5 hybrid photocatalyst since the residual strain and piezoelectric potential decreased. As a result, the TZO-4 hybrid photocatalyst with maximum strain has the strongest photocatalytic activity, and the photodegradation of MO solution is up to 99% after 90 min UV irradiation. Figure 4b further exhibits the photocatalytic performance of all samples, which indicates an obvious trend of continuous increase then a decrease from TZO-1 to TZO-5 hybrid photocatalyst. Compared with that of TZO-1, the photocatalytic performance of TZO-4 has increased more than 20%. However, it also reveals that the photocatalytic ability of ZnO/TiO_2 hybrid photocatalysts will not increase in an unlimited manner but will gradually maximize at a certain strain. Additionally, for the purpose of confirming the residual stress driven piezotronic effect on the photocatalytic performance of ZnO/TiO_2 hybrid photocatalysts, their photodegradation ability of MB under UV light irradiation was also studied

DOI: 10.1021/acsnano.5b07678
ACS Nano XXXX, XXX, XXX–XXX

(Figure 4c,d). As expected, the result is consistent with the above analysis, which also shows a continuously enhanced performance from TZO-1 to the sample of TZO-4 and a reverse trend from the TZO-4 to TZO-5 hybrid photocatalyst. Similarly, the TZO-4 hybrid phothocatalyst with maximum strain also has the best photodegradation performance and reaches 100% degradation of MB after 60 min under UV light irradiation. In addition, the photodegradation performance of TZO-4 has increased by 17% compared with the TZO-1 hybrid photocatalysts. All these results illuminated that the piezotronic effect can continuously enhance the photocatalytic performance driven bythe piezopotential under residual stress of ZnO/TiO_2 hybrid photocatalysts. More importantly, it is reasonable to speculate the extension that this strategy is universal for regulating the carriers' separation and transportation in semiconductors and is not accidental and limited.

A thermal stress induced internal strain was created by cooling the ZnO/TiO_2 hybrid photocatalysts from high temperature at different cooling rates. The expansion coefficient of ZnO monocrystalline nanoplatelets along the [001] direction is 4.3×10^{-6} K^{-1}, while it is 6.4×10^{-6} K^{-1} along the [100] direction, and that of TiO_2 nanoparticles is 9.0×10^{-6} K^{-1}, resulting in a different level of anisotropic compressive strain on ZnO monocrystalline nanoplatelets by the shell of TiO_2. Thus, as shown in Figure 5a, when the samples are cooled at different rates, piezoelectric potentials with different magnitude will be produced. To understand the influence of the piezotronic effect on the carrier transportation at the ZnO/TiO_2 interface, simplified band structure diagrams for ideal heterostructures are given in Figure 5b−d to better demonstrate the underlying working mechanism. The conduction band positions and the band gap energies of ZnO and TiO_2 were assumed to be the same, because the real difference between them is too small, about 0.04 eV.[36,37] The effects of interface states are ignored, and we represent electrochemical equilibrium between the solid and solution by matching the Fermi level with the solution H_2/H^+ level. The surface potential of TiO_2 was set to a value determined from flat band measurements assuming the interface states with the solution are unperturbed by the heterostructure. Upon UV illumination, electron−hole pairs are generated in ZnO monocrystalline nanoplatelets and TiO_2 nanoparticles, but a random motion of the charges results in a high recombination rate between the electrons and holes, reducing the photocatalytic efficiency severely (Figure 5b). Since the band structure is relatively flat without enough driving force to separate the electrons and holes, if there is a built-in potential caused by the piezoelectric effect at the interface, the electrons and holes would tend to move in opposite directions, which would greatly reduce the recombination rate at the surface. On one hand, when a compressive strain is applied to the ZnO monocrystalline along the *c*-axis, negative piezoelectric polarization charges are induced at the polar surface of the positive *c*-axis. These immobile ionic charges deplete free electrons near the semiconductor−semiconductor interface and therefore result in upward band bending, as shown in Figure 5c. When the electron−hole pairs are generated under UV light irradiation, they will be effectively separated immediately by introducing a strong local electric field across the interface, which can reduce the recombination rate and increase the carrier lifetime and density, thus enhancing the photocatalytic performance. Additionally, the induced negative piezopotential will become larger as the strain increases and the band will bend more, resulting in further improvement of the charge separation. On the other hand, the positive piezoelectric polarization charges are induced near the other polar surface of the negative *c*-axis, attracting free electrons toward the semiconductor−semiconductor interface and therefore resulting in downward band bending at the contact interface, as shown in Figure 5d. As a result, this situation is beneficial for electrons to transfer from the conduction band of ZnO to TiO_2 and holes to transfer from the valence band of TiO_2 to ZnO, while the transportation direction is opposite in the other interface of the heterojunction; therefore this synergy effect further enhances the photocatalytic performance through improving the charge separation by piezotornic effects.

CONCLUSIONS

In conclusion, we successfully developed an effective piezoelectric semiconductor-based hybrid photocatalyst by assembling TiO_2 nanoparticles on ZnO monocrystalline nanoplatelets and achieved piezopotential continuously enhanced photocatalysis. The piezopotential can be introduced and tuned by thermal stress on the piezoelectric material of ZnO monocrystalline nanoplatelets through cooling hybrid photocatalysts from high temperature to room temperature with different rates based on the mismatched thermal expansion coefficient of the two materials. Remarkably, the photocatalytic performance of ZnO/TiO_2 hybrid photocatalysts was significantly improved up to 20% by modulating the residual strain in the hybrid structure. The piezotronic effect can enhance the photocatalytic performance continuously in a wide range by effectively separating the photogenerated electrons and holes through engineering the band structure at heterojunction interfaces. It is thought that the piezotronic effect enhanced photocatalyst will provide a strategy for high-performance photocatalysis applications. Moreover, it broadens the scope of piezotronics and extends its potential applications in the fields of flexible electronics, flexible optoelectronics, and human−machine interfacing.

METHODS

Synthesis. Zinc acetate dihydrate ($Zn(CO_2CH_3)_2{\cdot}2H_2O$), tris(hydroxymethyl)aminomethane ($C_4H_{11}NO_3$, here referred to as TB), ethanol (CH_3CH_2OH), and titanium butoxide ($C_{16}H_{36}O_4Ti$) are all analytically pure without further treatment. ZnO monocrystalline nanoplatelets were synthesized through the hydrothermal method. Typically, the water solutions containing 0.2−1.0 M zinc acetate dihydrate and 0.3−1.0 M TB were prepared for ZnO nanoplatelet growth at 95 °C for 3 h in an oven. Finally, the precipitates were collected from the solution by centrifugation and sequentially washed with deionized water and ethanol several times and dried at 60 °C for 4 h.

ZnO/TiO_2 precursors were prepared by a simple coprecipitation method. A 0.15 mL amount of deionized (DI) water was dissolved in 10 mL of ethanol under vigorous magnetic stirring. A 0.5 g sample of ZnO monocrystalline nanoplatelets and 0.15 mL of titanium butoxide were dispersed into 10 mL of ethanol under ultrasound, which was then added into the above solution of DI water and ethanol. Then the mixed solution was stirred for 1 h to ensure complete reaction. After reaction, the products were collected from the solution by centrifugation, sequentially washed with ethanol several times, and dried at 60 °C for 4 h. The ZnO/TiO_2 precursors were sintered in a muffle furnace at 450 °C for 2 h and cooled to room temperature in a different process. The ZnO/TiO_2 products named TZO-1 were naturally cooled to room temperature in a muffle furnace, while the samples named TZO-2, TZO-3, and TZO-4 were cooled to room temperature in air, with ice and with liquid nitrogen, respectively. When the TZO-4 sample was sintered again at 200 °C in an oven for

DOI: 10.1021/acsnano.5b07678
ACS Nano XXXX, XXX, XXX−XXX

12 h and then naturally cooled to room temperature to relieve the stress, it was named TZO-5.

Characterization. XRD patterns of the powders were recorded on an X-ray diffraction spectrometer (Cu Kα, D8-Advance, Bruker AXS, Germany). Raman measurements were carried out using the LabRam HR Evolution system using the 532 nm line of an argon ion laser as the excitation source. The Micro-PL study was carried out using the 325 nm line of a He−Cd laser. A Hitachi S-8020 field-emission scanning electron microscope (FE-SEM) was used to characterize the morphology of the synthesized samples. The composition of ZnO/TiO_2 was analyzed by an energy-dispersion spectroscopy (EDS, Oxford link system) analyzer, which was attached to the SEM. The transmission electron microscopic (TEM) images were acquired with a FEI TECNAI F20 microscope operating at 200 kV. X-ray photoelectron spectroscopy was performed on an ESCALAB 250 instrument from Thermo Fisher Scientific, USA. The standard C 1s peak was used as a reference for correcting the shifts. UV−vis−NIR diffuse reflectance spectra were obtained by using a UV−vis−NIR spectrophotometer (UV-3600, Shimadzu) with an integrating sphere attachment in the range 200 to 800 nm and with $BaSO_4$ as reflectance standard. The performance of the piezoeletric nanogenerators was characterized using a conductive AFM system (MFP-3D from Asylum Research) with a conducting Pt-coated AFM probe that has a spring constant of 1.90 nN/nm and inverse optical lever sensitivity of 118.91 nm/V.

Photocatalytic Performance Measurement. The photocatalytic activity of ZnO monocrystalline nanoplatelets and the ZnO/TiO_2 hybrid photocatalyst was examined by the photodegradation of MO and MB in a photochemical reaction apparatus. In a typical experiment, 20 mL aqueous suspensions of MO (20 mg/L) and 100 mg of sample were placed in a 50 mL test tube. Twenty milliliter aqueous suspensions of MB (5 mg/L) and 30 mg of sample were placed in a 50 mL test tube. Prior to irradiation, the suspensions were magnetically stirred in the dark for 30 min to establish an adsorption/desorption equilibrium between the dye and the surface of the catalyst at room temperature. A 500 W mercury lamp with a maximum emission at 356 nm was used as the UV light source. An aliquot of the mixed solution was collected and centrifuged several times. At varied irradiation time intervals, the residual MO and MB concentration in the supernatant was analyzed by a multidetection microplate reader (BioTek Synergy HT, USA) at 465 and 664 nm, respectively.

ASSOCIATED CONTENT

Supporting Information

The Supporting Information is available free of charge on the ACS Publications website at DOI: 10.1021/acsnano.5b07678.

Additional information and figures, including experimental details, materials and method, and supplementary text (PDF)

AUTHOR INFORMATION

Corresponding Authors

*E-mail: qinyong@lzu.edu.cn.

*E-mail: zhong.wang@mse.gatech.edu.

Author Contributions

‡L. Wang and S. Liu contributed equally to this work.

Notes

The authors declare no competing financial interest.

ACKNOWLEDGMENTS

The authors acknowledge support from NSFC (Nos. 51322203, 51472111, 51302120), the National Program for Support of Top-notch Young Professionals, the "Thousands Talents" Program for pioneer researcher and his innovation team, China, and the Fundamental Research Funds for the Central Universities (No. lzujbky-2014-m02).

REFERENCES

(1) Zhou, P.; Yu, J.; Jaroniec, M. All-Solid-State Z-Scheme Photocatalytic Systems. *Adv. Mater.* **2014**, *26*, 4920−35.

(2) Hisatomi, T.; Kubota, J.; Domen, K. Recent Advances in Semiconductors for Photocatalytic and photoelectrochemical water splitting. *Chem. Soc. Rev.* **2014**, *43*, 7520−35.

(3) Li, Z.; Yao, C.; Yu, Y.; Cai, Z.; Wang, X. Highly Efficient Capillary Photoelectrochemical Water Splitting Ssing Cellulose Nanofiber-Templated TiO(2) Photoanodes. *Adv. Mater.* **2014**, *26*, 2110.

(4) Crossland, E. J.; Noel, N.; Sivaram, V.; Leijtens, T.; Alexander-Webber, J. A.; Snaith, H. J. Mesoporous TiO_2 Single Crystals Delivering Enhanced Mobility and Optoelectronic Device Performance. *Nature* **2013**, *495*, 215−9.

(5) Yu, Y.; Yin, X.; Kvit, A.; Wang, X. Evolution of Hollow TiO_2 Nanostructures *via* the Kirkendall Effect Driven by Cation Exchange with Enhanced Photoelectrochemical Performance. *Nano Lett.* **2014**, *14*, 2528−35.

(6) Hagfeldt, A.; Gratzel, M. Light-Induced Redox Reactions in Nanoctystalline Systems. *Chem. Rev.* **1995**, *95*, 49−68.

(7) Murdoch, M.; Waterhouse, G. I. N.; Nadeem, M. A.; Metson, J. B.; Keane, M. A.; Howe, R. F.; Llorca, J.; Idriss, H. The Effect of Gold Loading and Particle Size on Photocatalytic Hydrogen Production From Ethanol over Au/TiO_2 Nanoparticles. *Nat. Chem.* **2011**, *3*, 489−492.

(8) Tian, J.; Sang, Y.; Yu, G.; Jiang, H.; Mu, X.; Liu, H. A Bi_2 WO_6 -Based Hybrid Photocatalyst with Broad Spectrum Photocatalytic Properties under UV, Visible, and Near-Infrared Irradiation. *Adv. Mater.* **2013**, *25*, 5075−80.

(9) Sang, Y.; Zhao, Z.; Zhao, M.; Hao, P.; Leng, Y.; Liu, H. From UV to Near-Infrared, WS_2 Nanosheet: a Novel Photocatalyst for Full Solar Light Spectrum Photodegradation. *Adv. Mater.* **2015**, *27*, 363−9.

(10) Qu, Y.; Duan, X. Progress, Challenge and Perspective of Heterogeneous Photocatalysts. *Chem. Soc. Rev.* **2013**, *42*, 2568−80.

(11) Cheng, C.; Amini, A.; Zhu, C.; Xu, Z.; Song, H.; Wang, N. Enhanced Photocatalytic Performance of TiO_2-ZnO Hybrid Nanostructures. *Sci. Rep.* **2014**, *4*, 4181.

(12) Abdi, F. F.; Han, L.; Smets, A. H.; Zeman, M.; Dam, B.; van de Krol, R. Efficient Solar Water Splitting by Enhanced Charge Separation in a Bismuth Vanadate-Silicon Tandem Photoelectrode. *Nat. Commun.* **2013**, *4*, 2195.

(13) Kim, T. W.; Choi, K. S. Nanoporous BiVO4 Photoanodes with Dual-Layer Oxygen Evolution Catalysts for Solar Water Splitting. *Science* **2014**, *343*, 990−4.

(14) Esposito, D. V.; Levin, I.; Moffat, T. P.; Talin, A. A. H_2 Evolution at Si-Based Metal-Insulator-Semiconductor Photoelectrodes Enhanced by Inversion Channel Charge Collection and H Spillover. *Nat. Mater.* **2013**, *12*, 562−8.

(15) Li, X.; Li, Z.; Yang, J. Proposed Photosynthesis Method for Producing Hydrogen from Dissociated Water Molecules Using Incident Near-Infrared Light. *Phys. Rev. Lett.* **2014**, *112*, 018301.

(16) Shi, J.; Starr, M. B.; Wang, X. Band Structure Engineering at Heterojunction Interfaces *via* the Piezotronic Effect. *Adv. Mater.* **2012**, *24*, 4683−4691.

(17) Starr, M. B.; Shi, J.; Wang, X. Piezopotential-Driven Redox Reactions at the Surface of Piezoelectric Materials. *Angew. Chem., Int. Ed.* **2012**, *51*, 5962−6.

(18) Gao, Y.; Wang, Z. L. Electrostatic Potential in a Bent Piezoelectric Nanowire. The fundamental theory of nanogenerator and nanopiezotronics. *Nano Lett.* **2007**, *7*, 2499−2505.

(19) Wang, Z. L. Nanopiezotronics. *Adv. Mater.* **2007**, *19*, 889−892.

(20) Qin, Y.; Wang, X.; Wang, Z. L. Microfibre-Nanowire Hybrid Structure for Energy Scavenging. *Nature* **2008**, *451*, 809−U5.

(21) Wu, W.; Wen, X.; Wang, Z. L. Taxel-Addressable Matrix of Vertical-Nanowire Piezotronic Transistors for Active and Adaptive Tactile Imaging. *Science* **2013**, *340*, 952−7.

(22) Xu, S.; Qin, Y.; Xu, C.; Wei, Y.; Yang, R.; Wang, Z. L. Self-Powered Nanowire Devices. *Nat. Nanotechnol.* **2010**, *5*, 366−373.

(23) Zhang, Z.; Fan, R.; Shi, Z.; Yan, K.; Zhang, Z.; Wang, X.; Dou, S. Microstructure and Metal−Dielectric Transition Behaviour in a

DOI: 10.1021/acsnano.5b07678
ACS Nano XXXX, XXX, XXX−XXX

Percolative Al_2O_3−Fe Composite *via* Selective Reduction. *RSC Adv.* **2013**, *3*, 26110.
(24) Zhang, Z.-d.; Fan, R.-h.; Shi, Z.-c.; Pan, S.-b.; Yan, K.-l.; Sun, K.-n.; Zhang, J.-d.; Liu, X.-f.; Wang, X. L.; Dou, S. X. Tunable Negative Permittivity Behavior and Conductor−Insulator Transition in Dual Composites Prepared by Delective Reduction Reaction. *J. Mater. Chem. C* **2013**, *1*, 79−85.
(25) Wen, X.; Wu, W.; Ding, Y.; Wang, Z. L. Piezotronic Effect in Flexible Thin-Film Based Devices. *Adv. Mater.* **2013**, *25*, 3371−9.
(26) Shi, J.; Starr, M. B.; Xiang, H.; Hara, Y.; Anderson, M. A.; Seo, J. H.; Ma, Z.; Wang, X. Interface Engineering by Piezoelectric Potential in ZnO-Based Photoelectrochemical Anode. *Nano Lett.* **2011**, *11*, 5587−93.
(27) Li, J.; Qin, Y.; Kou, X.; He, H.; Song, D. Structure and Magnetic Properties of Cobalt Nanoplatelets. *Mater. Lett.* **2004**, *58*, 2506−2509.
(28) Li, J.; Qin, Y.; Kou, X.; Huang, J. The Microstructure and Magnetic Properties of Ni Nanoplatelets. *Nanotechnology* **2004**, *15*, 982−986.
(29) Tartakovskii, A. I.; Makhonin, M. N.; Sellers, I. R.; Cahill, J.; Andreev, A. D.; Whittaker, D. M.; Wells, J. P. R.; Fox, A. M.; Mowbray, D. J.; Skolnick, M. S.; et al. Effect of Thermal Annealing and Strain Engineering on the Fine Structure of Quantum Dot Excitons. *Phys. Rev. B: Condens. Matter Mater. Phys.* **2004**, *70*, 193303.
(30) Harbord, E.; Ota, Y.; Igarashi, Y.; Shirane, M.; Kumagai, N.; Ohkouchi, S.; Iwamoto, S.; Yorozu, S.; Arakawa, Y. Enhancement of Valence Band Mixing in Individual InAs/GaAs Quantum Dots by Rapid Thermal Annealing. *Jpn. J. Appl. Phys.* **2013**, *52*, 8.
(31) Shan, W.; Walukiewicz, W.; Ager, J. W.; Yu, K. M.; Zhang, Y.; Mao, S. S.; Kling, R.; Kirchner, C.; Waag, A. Pressure-Dependent Photoluminescence Study of ZnO Nanowires. *Appl. Phys. Lett.* **2005**, *86*, 3.
(32) Yang, S.; Tian, X.; Wang, L.; Wei, J.; Qi, K.; Li, X.; Xu, Z.; Wang, W.; Zhao, J.; Bai, X.; et al. In-Situ Optical Transmission Electron Microscope Study of Exciton Phonon Replicas in ZnO Nanowires by Cathodoluminescence. *Appl. Phys. Lett.* **2014**, *105*, 071901.
(33) Yang, Q.; Wang, W.; Xu, S.; Wang, Z. L. Enhancing Light Emission of ZnO Microwire-Based Diodes by Piezo-Phototronic Effect. *Nano Lett.* **2011**, *11*, 4012−7.
(34) Sahoo, S.; Sharma, G. L.; Katiyar, R. S. Raman Spectroscopy to Probe Residual Stress in ZnO Nanowire. *J. Raman Spectrosc.* **2012**, *43*, 72−75.
(35) Yan, B.; Chen, R.; Zhou, W.; Zhang, J.; Sun, H.; Gong, H.; Yu, T. Localized Suppression of Longitudinal-Optical-Phonon-Exciton Coupling in Bent ZnO Nanowires. *Nanotechnology* **2010**, *21*, 445706.
(36) Kavan, L.; Gratzel, M.; Gilbert, S. E.; Klemenz, C.; Scheel, H. J. Electrochemical and Photoelectrochemical Investigation of Single-Crystal Anatase. *J. Am. Chem. Soc.* **1996**, *118*, 6716−6723.
(37) Cardona, M. Optical Properties and Band Structure of $SrTiO_3$ and $BaTiO_3$. *Phys. Rev.* **1965**, *140*, A651.

DOI: 10.1021/acsnano.5b07678
ACS Nano XXXX, XXX, XXX−XXX